Journal of Physics: Conference Series **336** (2011) 012022 doi:10.1088/1742-6596/336/1/012022

Neutron star structure with hyperons and quarks

H-J Schulze

INFN Sezione di Catania, Dipartimento di Fisica, Via Santa Sofia 64, I-95123 Catania, Italy

Abstract. The high-density nuclear equation of state within the Brueckner-Hartree-Fock approach is discussed. Particular attention is paid to the effects of nucleonic three-body forces, the presence of hyperons, the joining with an eventual quark matter phase, and the extension to finite temperature. The resulting properties of neutron stars, in particular the mass-radius relation, are determined. It turns out that in this approach stars heavier than about 1.4 solar masses contain necessarily quark matter.

1. Introduction

During the last decades the increasing interest for the equation of state (EOS) of nuclear matter has stimulated a lot of theoretical activity. The properties of nuclear matter at high density and large isospin asymmetry are relevant for astrophysical objects, i.e., supernovae and neutron stars (NS). In particular, the structure of a NS is very sensitive to the compressibility and the symmetry energy. The NS mass, measured in binary systems, has been proposed as a constraint for the EOS of nuclear matter [1, 2, 3].

One of the most advanced microscopic approaches to the EOS of nuclear matter is the Brueckner theory. In recent years, it has made solid progress regarding the convergence of the underlying Brueckner-Bethe-Goldstone (BBG) expansion, the addition of microscopic three-body forces (TBF), the inclusion of hyperons, and the extension to finite temperature. These issues are reviewed in this contribution and results for NS structure based on the resulting EOS of dense hadronic matter are presented. Doing so, it turns out necessary to consider the transition to quark matter in the interior of sufficiently massive stars, which will also be discussed in detail.

2. Brueckner theory

The nonrelativistic BBG expansion for the energy of nuclear matter E/A can be cast as a power series in terms of the number of hole lines contained in the corresponding diagrams, which amounts to a density power expansion [4]. The two hole-line truncation is named the Brueckner-Hartree-Fock (BHF) approximation. At this order the energy E_2 is very much affected by the choice of the auxiliary single-particle (s.p.) potential. But, adding the three-hole line contributions E_3, the resulting EOS is almost insensitive to the choice of the auxiliary potential, and very close to the result E_2 with the continuous choice of the s.p. potential [5].

In spite of this satisfactory convergence, the saturation density misses the empirical value $\rho_0 \approx 0.17$ fm^{-3} extracted from the central density of heavy nuclei. This confirms the belief that the concept of a many-nucleon system interacting via only two-body forces is not adequate to describe nuclear matter, especially at high density. To this purpose three-body forces have to be taken into account.

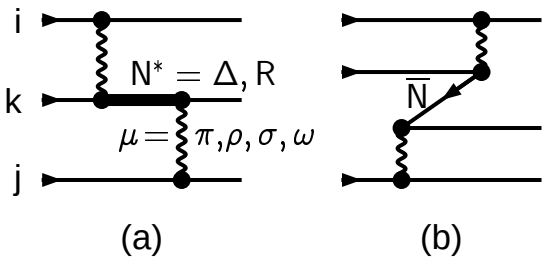

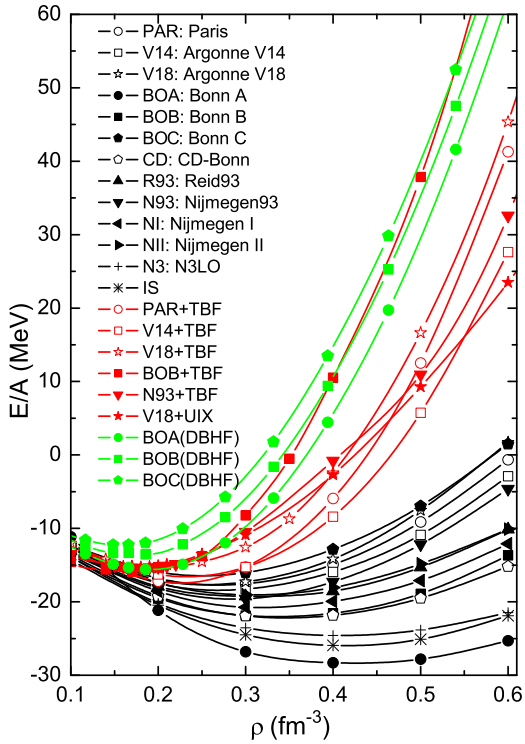

Figure 1. (Color online) Above: Diagrams contributing to the microscopic TBF. Right: Energy per nucleon of symmetric nuclear matter employing different potentials and TBF.

3. Three-body forces

The microscopic TBF of Refs. [6] are based on meson-exchange mechanisms accompanied by the excitation of nucleonic resonances, as represented by the diagram figure 1(a), namely the excitation of the isobar $\Delta(1232)$ resonance via the exchange of light (π,ρ) mesons, the lowest non-isobar nucleon resonance $N^*(1440)$ excited mainly by heavy meson (σ,ω) exchanges, as well as the generation of a virtual $N\bar{N}$ pair [diagram (b)]. The meson-exchange parameters of this model are chosen compatible with the underlying nucleon-nucleon (NN) potential. A second class of TBF widely used in the literature are the phenomenological Urbana TBF [7], which consider only $\Delta(1232)$ exchange and add a phenomenological repulsive scalar contribution.

The effect of these TBF is a stiffening of the EOS and a consequent remarkable improvement of the saturation properties of symmetric nuclear matter [8], as shown in figure 1 (right) for the EOS bases on different modern NN potentials with (red curves) and without (black curves) TBF.

4. Neutron star structure

In order to study the effects of different TBF on NS structure, the composition and the EOS of charge-neutral matter consisting of neutrons, protons, and leptons (e^-, μ^-) in beta equilibrium are calculated in the following standard way [9]: The Brueckner calculation yields the energy density of baryon/lepton matter as a function of the different partial densities,

$$\varepsilon(\rho_n,\rho_p,\rho_e,\rho_\mu) = (\rho_n m_n + \rho_p m_p) + (\rho_n+\rho_p)\frac{E}{A}(\rho_n,\rho_p) + \varepsilon_e + \varepsilon_\mu \,, \tag{1}$$

where $\varepsilon_{e,\mu}$ are the contributions of the non-interacting leptons. The various chemical potentials (of the species $i = n, p, e, \mu$) can then be computed straightforwardly,

$$\mu_i = \frac{\partial \varepsilon}{\partial \rho_i} \,, \tag{2}$$

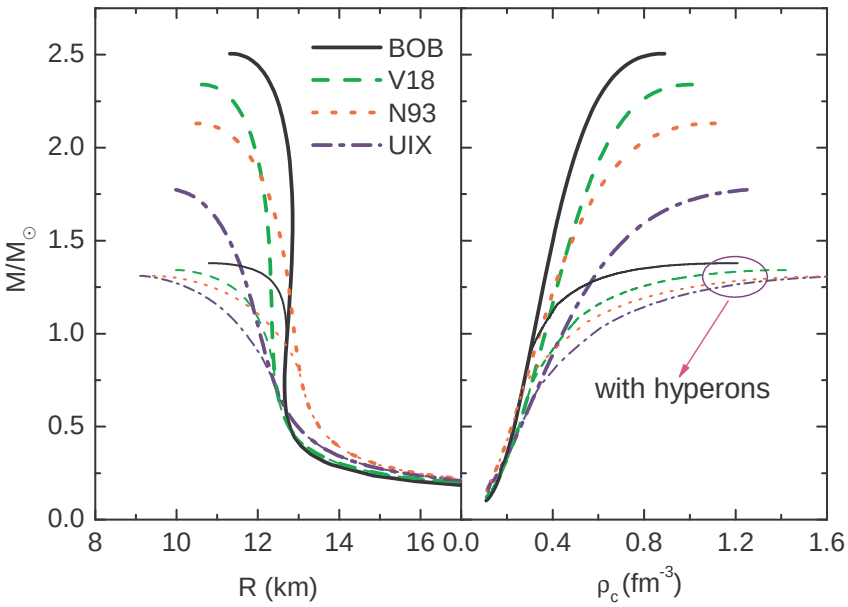

Figure 2. (Color online) The NS gravitational mass (in units of solar mass $M_\odot$) vs. the radius (left panel) and the central baryon density ρ_c (right panel) for different hadronic EOSs with (thin curves) or without (thick curves) hyperons.

and the equations for beta equilibrium and charge neutrality (b_i and q_i denoting baryon number and charge of species i),

$$\mu_i = b_i\mu_n - q_i\mu_e \quad , \quad \sum_i \rho_i q_i = 0 \, , \tag{3}$$

allow to determine the equilibrium composition $\{\rho_i(\rho)\}$ at given baryon density $\rho = \rho_n + \rho_p$ and finally the EOS,

$$p(\rho) = \rho^2 \frac{d}{d\rho}\frac{\varepsilon(\{\rho_i(\rho)\})}{\rho} = \rho\frac{d\varepsilon}{d\rho} - \varepsilon = \rho\mu_n - \varepsilon \, . \tag{4}$$

In order to calculate the mass-radius relation, one has then to solve the well-known Tolman-Oppenheimer-Volkov equations [9],

$$\frac{dp}{dr} = -\frac{Gm}{r^2}\frac{(\varepsilon+p)(1+4\pi r^3 p/m)}{1-2Gm/r} \quad , \quad \frac{dm}{dr} = 4\pi r^2 \varepsilon \, . \tag{5}$$

The solutions provide information on the interior structure of a star, $\rho_i(r)$, as well as the mass-radius relation, $M(R)$.

The results obtained with different potentials+compatible TBF are shown in figure 2 (thick curves). One notices maximum masses ranging from about 1.8 $M_\odot$ (UIX) up to about 2.5 $M_\odot$ (BOB), reflecting the current theoretical uncertainty regarding nuclear TBF. However, these results should be considered as only provisory, since it is well known that the inclusion of hyperons or quark matter may strongly affect the structure of the star, in particular reducing substantially the maximum mass. This is discussed now in more detail.

5. Hyperons in nuclear matter

While at moderate densities $\rho \approx \rho_0$ the matter inside a NS consists only of nucleons and leptons, at higher densities several other species of particles, like Λ, Σ, and Ξ hyperons, may appear due to the fast rise of the baryon chemical potentials with density. In the following it is assumed that a baryonic description of nuclear matter holds up to those densities encountered in the core of NS, and the hyperon degrees of freedom are included within the BHF approximation [10, 11].

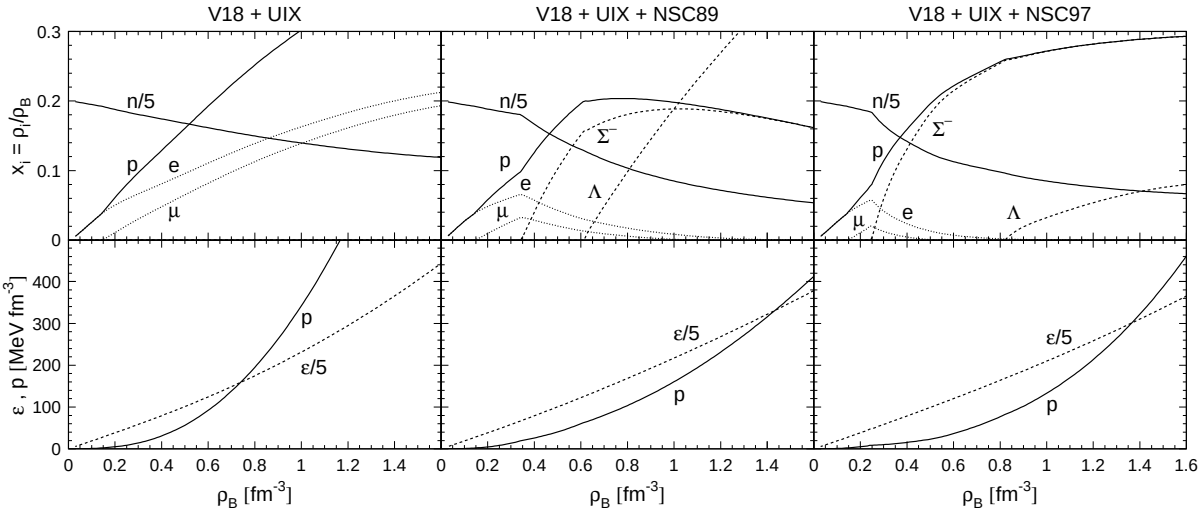

Figure 3. The composition and EOS of asymmetric and beta-stable hypernuclear matter.

To this purpose, one requires nucleon-hyperon (NY) and hyperon-hyperon (YY) potentials. In our work the Nijmegen soft-core NY potentials NSC89 [12] or NSC97f [13] are used, which are fitted to the available experimental NY scattering data, together with the nucleonic forces + TBF introduced before. With the NN and NY potentials, the various G matrices are evaluated by solving numerically the Bethe-Goldstone equation, written in operatorial form as

$$G_{ab}[W] = V_{ab} + \sum_c \sum_{p,p'} V_{ac} \Big| pp' \Big\rangle \frac{Q_c}{W - E_c + i\varepsilon} \Big\langle pp' \Big| G_{cb}[W] \,, \tag{6}$$

where the indices a, b, c indicate pairs of baryons and the Pauli operator Q_c and energy E_c determine the propagation of intermediate baryon pairs. In a given baryon-baryon channel $c = (12)$ one has

$$Q_{(12)} = [1 - n_1(k_1)][1 - n_2(k_2)] \,, \tag{7}$$
$$E_{(12)} = m_1 + m_2 + e_1(k_1) + e_2(k_2) \tag{8}$$

with the s.p. energy $e_i(k) = k^2/2m_i + U_i(k)$ and the distribution function $n_i(k) = \theta(k_F^{(i)} - k)$. The various s.p. potentials within the continuous choice are given by

$$U_1(k_1) = \mathrm{Re} \sum_{2=n,p,\Lambda,\Sigma} \sum_{k_2} n_2(k_2) \Big\langle k_1 k_2 \Big| G_{(12)(12)}[E_{(12)}] \Big| k_1 k_2 \Big\rangle_A \,, \tag{9}$$

where k_i generally denote momentum and spin. Once the different s.p. potentials are known, the total nonrelativistic baryonic energy density, the EOS, and NS structure can be computed as described before, now making allowance for the species $i = n, p, \Lambda, \Sigma^-, e^-, \mu^-$.

Figure 3 shows the composition of the resulting beta-stable and charge-neutral asymmetric nuclear matter containing hyperons. One observes rather low Σ^- onset densities of about $(2-3)\rho_0$. Also, an almost equal percentage of nucleons and hyperons is present in the stellar core at high densities, and thus the inclusion of hyperons produces a much softer EOS.

The consequences for the structure of NS are illustrated by the thin curves in figure 2. One notes that while the purely nucleonic EOSs yielded quite different maximum masses, the presence of hyperons equalizes in a self-regulating way the results, leading now to maximum

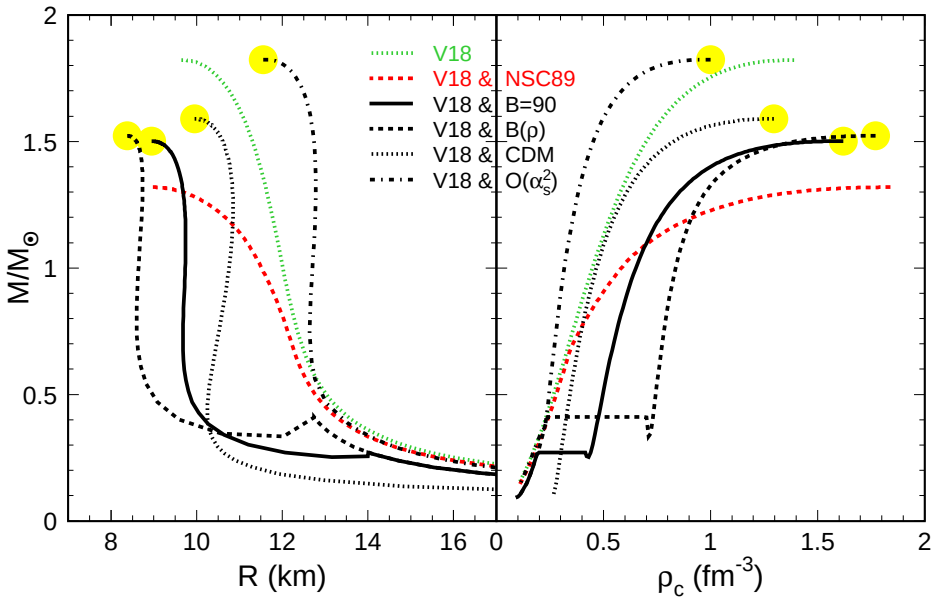

Figure 4. (Color online) The mass-radius and mass-central density relations for different hybrid neutron stars.

masses of 1.3–1.4 solar masses for all the nuclear TBF. This surprising result is due to the strong softening of the baryonic EOS when including hyperons as additional degrees of freedom, and one does not expect substantial changes when introducing refinements of the theoretical framework, such as hyperon-hyperon potentials, hyperonic TBF [14], relativistic corrections, etc.. The only remaining possibility in order to reach larger maximum masses appears the transition to another phase of dense (quark) matter inside the star [15, 16, 17, 18].

6. Quark matter

Unfortunately, the current theoretical description of quark matter is burdened with large uncertainties, seriously limiting the predictive power of any theoretical approach at high baryonic density. For the time being one can therefore only resort to phenomenological models for the quark matter EOS and try to constrain them as well as possible by the few experimental information on high-density baryonic matter. One important condition is due to the fact that certainly in symmetric nuclear matter no phase transition is observed below $\rho \approx 3\rho_0$.

The MIT bag model [19] provides a simple example for the description of the bulk properties of uniform quark matter, deconfined from the beta-stable hadronic matter mentioned in the previous section. The energy density of the $f = u, d, s$ quark gas can be expressed as a sum of the kinetic term and the one-gluon-exchange term [20, 21] proportional to the QCD coupling constant α_s,

$$\varepsilon_Q = B + \sum_f \varepsilon_f \,, \tag{10}$$

$$\varepsilon_f(\rho_f) = \frac{3m_f^4}{8\pi^2}\left[\left(2x_f^3 + x_f\right) y_f - \operatorname{arsinh} x_f\right] - \alpha_s \frac{m_f^4}{\pi^3}\left[x_f^4 - \frac{3}{2}\left(x_f y_f - \operatorname{arsinh} x_f\right)^2\right], \tag{11}$$

where m_f is the f current quark mass, $x_f = k_F^{(f)}/m_f$, and $y_f = \sqrt{1+x_f^2} = E_F^{(f)}/m_f$. The baryon number density of f quarks is $\rho_f = {k_F^{(f)}}^3/3\pi^2$, and B is the energy density difference between the perturbative vacuum and the true vacuum, i.e., the bag "constant."

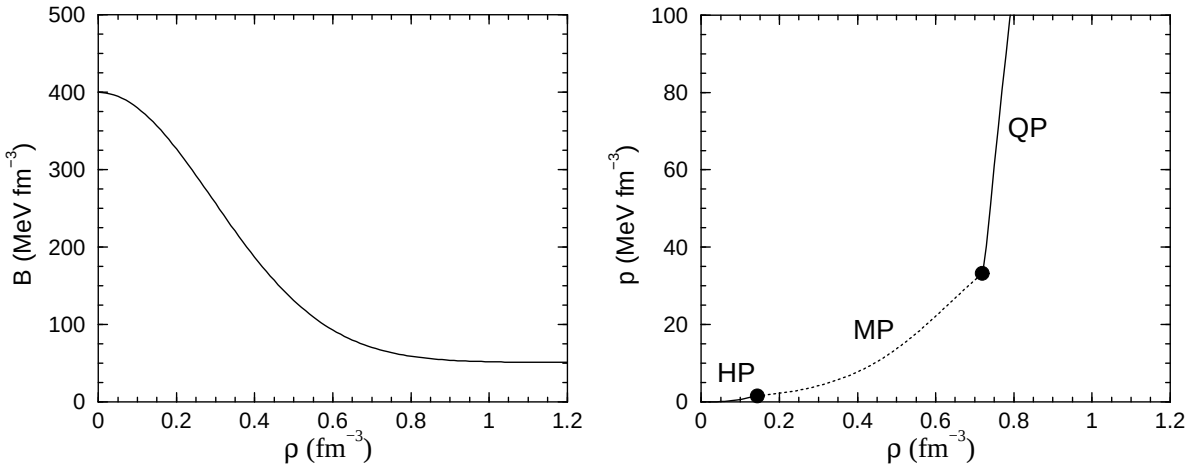

Figure 5. Left: Bag parameter B versus baryon number density. Right: EOS including both hadronic and quark components. The mixed phase region of quarks and hadrons (MP) is bordered by two dots, while HP and QP label the pure hadron and quark phases.

It has been found [15, 22] that within the MIT bag model (without color superconductivity) with a density-independent bag constant B, the maximum mass of a NS cannot exceed a value of about 1.6 solar masses. Indeed, the maximum mass increases as the value of B decreases, but too small values of B are incompatible with a hadron-quark transition density $\rho \gtrsim (2-3)\rho_0$ in nearly symmetric nuclear matter, as demanded by heavy-ion collision phenomenology.

In order to overcome these restrictions of the model, one can introduce an empirical density-dependent bag parameter $B(\rho)$, and this approach was followed in Refs. [15, 16, 17]. This allows one to lower the value of B at large density, providing a stiffer QM EOS and increasing the value of the maximum mass, while at the same time still fulfilling the condition of no phase transition below $\rho \approx 3\rho_0$ in symmetric nuclear matter. The following results are based on the MIT model using either a constant value of the bag parameter, $B = 100$ MeV/fm^{-3}, or a Gaussian parametrization for the density dependence,

$$B(\rho) = B_\infty + (B_0 - B_\infty) \exp\left[-\beta\Big(\frac{\rho}{\rho_0}\Big)^2\right] \tag{12}$$

with $B_\infty = 50$ MeV/fm^3, $B_0 = 400$ MeV/fm^3, and $\beta = 0.17$, displayed in figure 5 (left panel).

In the beta-stable pure quark phase, the individual quark chemical potentials are fixed by Eq. (3) with $b_q = 1/3$, which implies

$$\mu_s = \mu_d = \mu_u + \mu_l \,. \tag{13}$$

The charge neutrality condition and the total baryon number conservation read

$$0 = 2\rho_u - \rho_d - \rho_s - \rho_l \,, \tag{14}$$

$$\rho = \rho_u + \rho_d + \rho_s \,. \tag{15}$$

These equations determine the composition $\rho_f(\rho)$ and the pressure of the QM phase,

$$p_Q(\rho) = \rho^2 \frac{d(\varepsilon_Q/\rho)}{d\rho} \,, \tag{16}$$

which can be used together with the pressure of the hadronic phase to determine the phase transition using a Maxwell construction (MC), i.e., equating baryon chemical potentials and pressures of the two phases.

The corresponding results for the structure of hybrid NS are shown in figure 4 (black curves), displaying mass-radius and mass-central density relations. It is evident that the most striking effect of the inclusion of quark matter is the increase of the maximum mass relative to the hyperon star, now reaching about 1.5 $M_\odot$ with the MIT models with a bag constant $B = 100$ MeV/fm^{-3} or with $B(\rho)$, about 1.6 $M_\odot$ with the more sophisticated color dielectric model (CDM) [17, 23], and about 1.8 $M_\odot$ in a recent O(α_s^2) calculation [18].

7. Hadron-quark phase transition

A more sophisticated model for the phase transition between hadronic and quark phase inside the star is the Gibbs (Glendenning) construction [24], which determines a range of baryon density where both phases coexist as a mixed phase (MP). The essential point of this procedure is that both the hadron and the quark phase are allowed to be separately charged, still preserving the total charge neutrality. The chemical potentials of the different species are related to each other satisfying chemical and beta stability, Eq. (3), while the pressure is the same in the two phases to ensure mechanical stability,

$$p_H(\mu_e, \mu_n) = p_Q(\mu_e, \mu_n) = p_M(\mu_n) \, . \tag{17}$$

The equation for global charge neutrality involving the charge densities q_H and q_Q,

$$0 \;=\; \chi q_Q + (1-\chi) q_H \, , \tag{18}$$

determines the additional parameter χ, the volume fraction occupied by quark matter in the MP. From this, the baryon density ρ_M and the energy density ε_M of the MP can be calculated:

$$\rho_M \;=\; \chi\rho_Q + (1-\chi)\rho_H \, , \tag{19}$$

$$\varepsilon_M \;=\; \chi\varepsilon_Q + (1-\chi)\varepsilon_H \, . \tag{20}$$

The EOS resulting from this procedure is shown in figure 5 (right panel) for the MIT model, where the pure hadron, mixed, and pure quark matter portions are indicated. The MP begins actually at a quite low density around ρ_0 and persists throughout a wide range of baryon density.

As a further refinement, surface and Coulomb energies in the hadron-quark MP may be taken into account [25, 26], so that charge and baryon number density are no more uniform, but the MP can have exotic shapes called pasta structures (for a review, see Ref. [27]). As a result, the broad density region of the MP in the bulk Gibbs (BG) calculation described before is considerably reduced and the EOS approaches the one given by the MC [27].

Within a Wigner-Seitz approximation the whole space is divided into equivalent cells with a given geometrical symmetry, sphere for three dimensions (3D), cylinder for 2D, and slab for 1D. In each cell the quark and hadron phases are spatially separated by a sharp boundary with surface S and the surface energy is taken into account with a surface tension parameter σ (a typical value is $\sigma = 40$ MeV/fm^2). The energy density of the MP is then written as

$$\varepsilon = \frac{1}{V_W}\left[\int_{V_H} d\boldsymbol{r}\, \varepsilon_H(\boldsymbol{r}) + \int_{V_Q} d\boldsymbol{r}\, \varepsilon_Q(\boldsymbol{r}) + \int_{V_W} d\boldsymbol{r}\left(\varepsilon_e(\boldsymbol{r}) + \frac{[\nabla\phi(\boldsymbol{r})]^2}{8\pi e^2}\right) + \sigma S\right] , \tag{21}$$

where the volume of the Wigner-Seitz cell is $V_W = V_H + V_Q$. ϕ is the Coulomb potential and ε_H, ε_Q, and ε_e are energy densities of hadrons, quarks, and electrons, respectively, which are

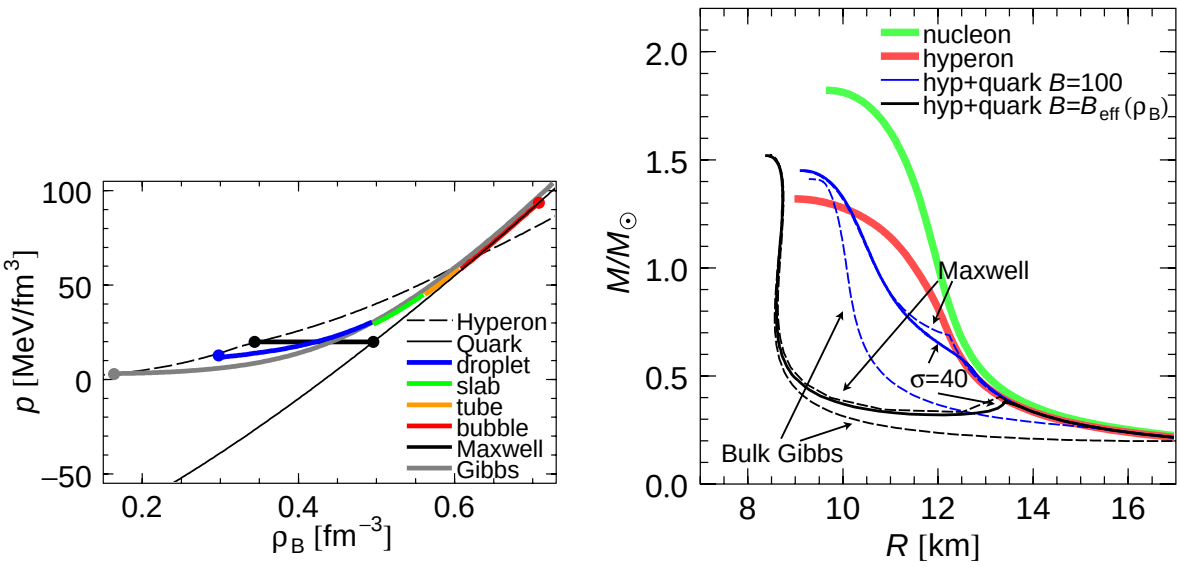

Figure 6. (Color online) Left: The pressure of the MP (thick curves) in comparison with the pure hadron and quark phases (thin curves), and the MC (black) and BG (gray) calculations. Right: NS mass-radius relations for different EOS and three different phase transition constructions. For the hybrid stars (blue and black curves), the dashed lines indicate the Maxwell (upper curves) or bulk Gibbs (lower curves) constructions and the solid lines the MP of the full calculation.

functions of local densities of $n, p, \Lambda, \Sigma^-, u, d, s, e$. For ε_H the BHF energy density is used and for the quark phase the MIT bag model introduced before. For a given baryon density ρ the optimum dimensionality of the cell, the cell size R_W, the lump size R, and the density profile of each component are searched for to minimize the energy density.

Figure 6 (left panel) compares the resulting EOS $p(\rho)$ with that of the pure hadron and quark phases. The thick black curve indicates the case of the MC, while the colored lines indicate the MP in its various geometric realizations, starting with quark droplets and terminating with quark bubbles. The charge screening effect tends to make matter locally charge neutral to reduce the Coulomb interaction energy. Combined with the surface tension, it renders the non-uniform structures mechanically less stable and limits the density region of the MP [27]. The structure and the composition of the MP are very different from those of the MC. In particular, although a relevant hyperon (Σ^-) fraction is present in the MC case, it is completely suppressed in the full calculation, because the hadron phase is allowed to be positively charged in the MP.

Figure 6 (right panel) compares the mass-radius relations obtained with the different models. The purely nucleonic EOS (thick green curve) yields a maximum NS mass of about $1.82\,M_\odot$, which is reduced to $1.32\,M_\odot$ when allowing the presence of hyperons (thick red curve). The inclusion of quark matter within the MIT model augments the maximum mass of hybrid stars to about $1.5\,M_\odot$, independently of the phase transition construction that is used: For the $B(\rho)$ model the maximum mass is $1.52\,M_\odot$, practically independent of the kind of phase transition, whereas for the $B = 100$ MeV/fm^{-3} model there is a slight variation of $M = 1.45, 1.45, 1.41\,M_\odot$ for the Maxwell, mixed, and bulk construction.

Whereas the maximum masses are practically independent of the phase transition construction, there are large differences for the internal composition of the star. This is illustrated in figure 7, which shows the total energy density, pressure, and particle fractions as a function of the radial coordinate for a $1.4\,M_\odot$ NS. One observes with the BG construction (left panel) a

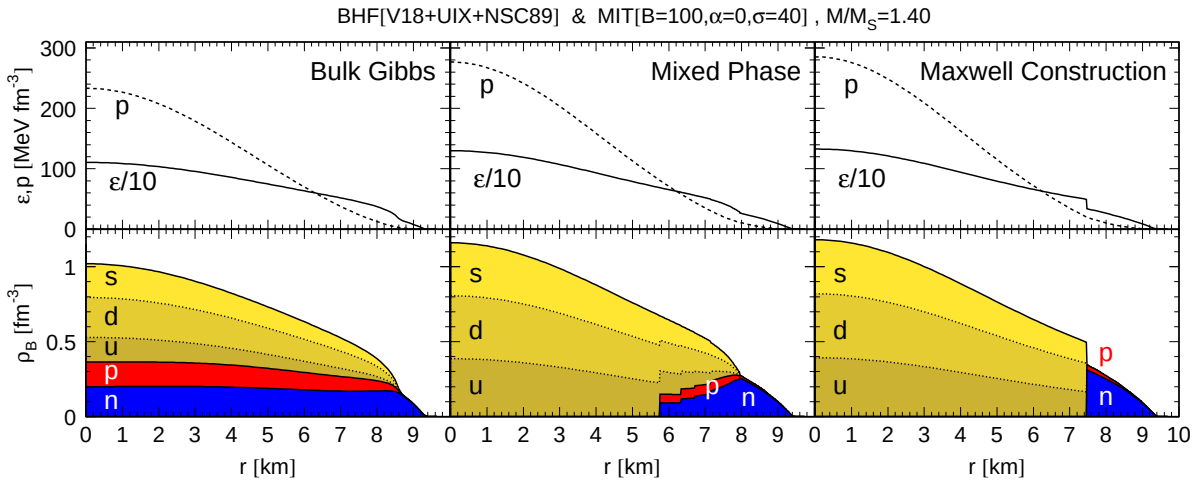

Figure 7. (Color online) Internal structure of a 1.4 $M_\odot$ NS obtained with the BG construction (left panel), the MP of the full calculation (central panel), and the MC (right panel). The upper panels show total energy density and pressure and the lower panels the overall particle fractions as functions of the radial coordinate of the star.

coexistence of hadrons and quarks in a significant range of the star, whereas with the MC (right panel) an abrupt transition involving a discontinuous jump of energy and baryon density occurs at a distance $r \approx 7.5$ km from the center of the star. The MP with the full calculation (central panel) lies between the two extreme cases, hadrons and quarks coexisting in a smaller range than in the BG case.

8. EOS at finite temperature: Protoneutron stars

A natural extension of the BHF formalism at zero temperature is the theoretical modeling of a protoneutron star (PNS), which represents the typical stellar state for some tens of seconds after supernova collapse, during which the system first deleptonizes and heats up the interior of the star in the process, before beginning to cool down by further neutrino diffusion [28].

We do not perform dynamical simulations, but focus on the consistent construction of the temperature-dependent nuclear EOS and the evaluation of its basic consequences during the prominent PNS stage [29, 30, 31, 32]. We therefore assume strongly idealized, static temperature and lepton-trapping profiles representing this environment, namely constant lepton fractions $Y_e \equiv x_e + x_{\nu_e} = 0.4$, $Y_\mu = 0$ and a constant entropy per baryon throughout the star, and investigate the sensitivity of the results to the chosen value of entropy S/A [33, 34].

The finite-temperature extension of the Bethe-Goldstone equation [4, 35, 36] consists in replacing the distribution function $n_i(k)$ appearing in the Pauli operator Q_c in Eq. (7) and the s.p. potential, Eq. (9), by the Fermi distribution $n_i(k) = (e^{[e_i(k)-\tilde{\mu}_i]/T} + 1)^{-1}$. For given partial densities ρ_i $(i = n, p, \Lambda, \Sigma)$ and temperature T, Eqs. (6) and (9) have to be solved self-consistently along with the equations for the auxiliary chemical potentials $\tilde{\mu}_i$,

$$\rho_i = \sum_k n_i(k) \, . \tag{22}$$

Once the different s.p. potentials for the species $i = n, p, \Lambda, \Sigma^-$ are known, the free energy density of hypernuclear matter has the following simplified expression

$$f = \sum_i \left[\sum_k n_i(k) \left(\frac{k^2}{2m_i} + \frac{1}{2} U_i(k) \right) - T s_i \right] \, , \tag{23}$$

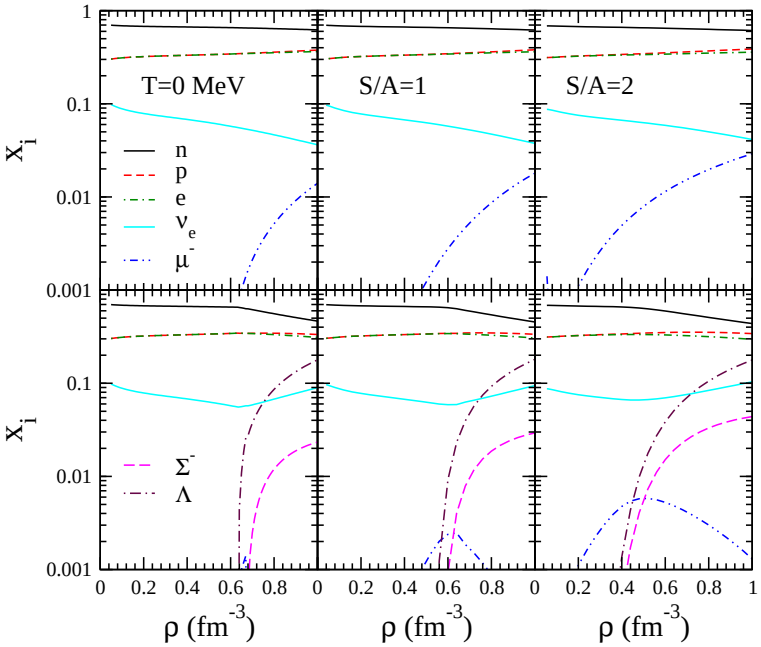

Figure 8. (Color online) Relative particle fractions as functions of baryon density in neutrino-trapped beta-equilibrated matter at entropies $S/A = 0, 1, 2$ without (upper panels) and with (lower panels) hyperons.

where

$$s_i = -\sum_k \Big(n_i(k) \ln n_i(k) + [1 - n_i(k)] \ln[1 - n_i(k)] \Big) \tag{24}$$

is the entropy density for component i treated as a free gas with s.p. spectrum $e_i(k)$ [4, 36]. A further simplification can be achieved by disregarding the effects of finite temperature on the s.p. potentials U_i, and using the $T = 0$ results in order to speed up the calculations (frozen correlations approximation) [29, 30, 32].

All thermodynamic quantities of interest can then be computed from the free energy density, Eq. (23); namely, the 'true' chemical potentials μ_i, pressure p, entropy density s, and internal energy density ε read as

$$\mu_i = \frac{\partial f}{\partial \rho_i} , \tag{25}$$

$$p = \rho^2 \frac{\partial (f/\rho)}{\partial \rho} = \sum_i \mu_i \rho_i - f , \tag{26}$$

$$s = -\frac{\partial f}{\partial T} , \tag{27}$$

$$\varepsilon = f + Ts . \tag{28}$$

As an illustration, figure 8 shows the particle fractions at entropies $S/A = 0, 1, 2$ in beta-stable trapped matter [32]. One observes the following qualitative features: (i) Finite temperature removes any particle thresholds, i.e., hyperons and leptons become more and more abundant at low densities with rising temperature/entropy. (ii) Hyperon fractions are lower in trapped matter than in untrapped matter, in particular the Σ^- is strongly suppressed, because due to the trapping condition it cannot easily replace the electron as is the case in untrapped matter. These features have direct consequences for the EOS $p(\varepsilon)$: For purely nucleonic matter the effects of trapping and temperature are not very large, but both soften the EOS. On the contrary, hyperons soften the EOS of untrapped matter much more than that of trapped matter, due to

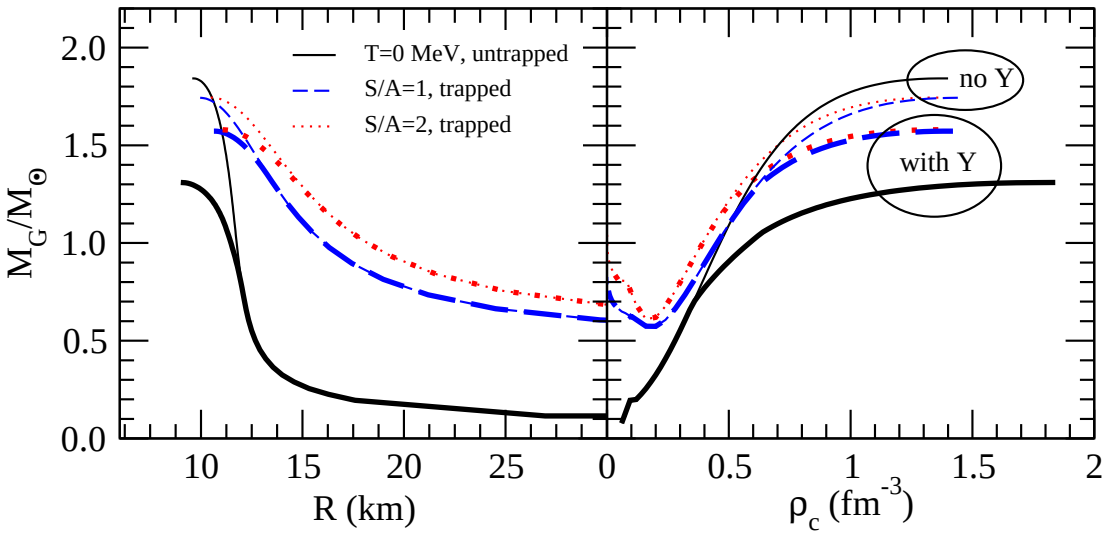

Figure 9. (Color online) Gravitational mass as a function of radius (left panel) and central baryon density (right panel) for cold NSs (solid curves) and neutrino-trapped PNSs at entropies $S/A = 1, 2$ (broken curves). The thick (thin) curves describe configurations with (without) hyperons.

their higher concentration in the former. Altogether, finite entropy and in particular trapping affect hyperon-rich matter much more (and in an opposite sense) than nuclear matter.

The relation $p(\varepsilon)$ as input to Eq. (5) determines directly the mass – radius relations of (P)NSs shown in figure 9 (left panel). One observes for nucleonic stars a slight reduction of the maximum mass (from about 1.84 $M_\odot$ to 1.74 $M_\odot$) due to trapping and finite temperature, while for hyperon stars both trapping and also finite temperature increase notably the maximum mass (from about 1.31 $M_\odot$ to 1.58 $M_\odot$). The latter feature would permit a delayed collapse phenomenon, as is usually found for hyperon stars [28, 33, 34, 37]. However, this conclusion is rather academic, because the maximum mass of hyperon stars is 1.31 $M_\odot$ in this approach, so that most observed NSs [3] would actually be hybrid stars involving a transition to quark matter in the interior, as pointed out before. This is also pinpointed by the mass – central density relations, displayed in figure 9 (right panel), which shows for hyperon stars central densities up to about 10 ρ_0, where a realistic description of stellar matter should necessarily include quark matter degrees of freedom.

9. Conclusions

This contribution reported the theoretical description of hypernuclear matter in the BHF approach and the application to NS structure calculation. The important role of TBF at high density was pointed out, which is, however, strongly compensated by the inclusion of hyperons. The resulting hadronic NS have maximum masses of less than about $1.4\,M_\odot$, and the presence of quark matter inside the star is required in order to reach larger values.

It remains to be seen which values of the maximum mass can be reached with more sophisticated quark matter models in the future, in particular with respect to the recent claim of discovery of a two solar mass NS [38].

Acknowledgments

Many collaborators have contributed to the work described here. In particular, M Baldo, G F Burgio, J Cugnon, A Lejeune, A Li, Z H Li, U Lombardo, C Maieron, T Maruyama, A Polls, A Ramos, T Tatsumi, I Vidaña, X R Zhou, and W Zuo.

References

[1] Glendenning N K 2000 *Compact Stars, Nuclear Physics, Particle Physics, and General Relativity*, 2nd ed. (Springer, New York)
[2] Haensel P, Potekhin A Y, and Yakovlev D G 2007 *Neutron Stars 1* (Springer, New York)
[3] Lattimer J M and Prakash M 2007 *Phys. Rep.* **442** 109
[4] Baldo M 1999 *Nuclear Methods and the Nuclear Equation of State*, *International Review of Nuclear Physics*, Vol. 8 (World Scientific, Singapore)
[5] Song H Q, Baldo M, Giansiracusa G, and Lombardo U 1998 *Phys. Rev. Lett.* **81** 1584; Baldo M, Fiasconaro A, Song H Q, Giansiracusa G, and Lombardo U 2001 *Phys. Rev. C* **65** 017303
[6] Coon S A, Scadron M D, McNamee P C, Barrett B R, Blatt D W E, and McKellar B H J 1979 *Nucl. Phys. A* **317** 242; Grangé P, Lejeune A, Martzolff M, and Mathiot J-F 1989 *Phys. Rev. C* **40** 1040; Zuo W, Lejeune A, Lombardo U, and Mathiot J-F 2002 *Nucl. Phys. A* **706** 418; Li Z H, Lombardo U, Schulze H-J, and Zuo W 2008 *Phys. Rev. C* **77** 034316; Li Z H and Schulze H-J 2008 *Phys. Rev. C* **78** 028801
[7] Pudliner B S, Pandharipande V R, Carlson J, Pieper S C, and Wiringa R B, 1997 *Phys. Rev. C* **56** 1720; Zhou X R, Burgio G F, Lombardo U, Schulze H-J, and Zuo W 2004 *Phys. Rev. C* **69** 018801
[8] Li Z H, Lombardo U, Schulze H-J, Zuo W, Chen L W, and Ma H R 2006 *Phys. Rev. C* **74** 047304
[9] Shapiro S and Teukolsky S A 2000 *Black Holes, White Dwarfs, and Neutron Stars* (John Wiley & Sons, New York)
[10] Schulze H-J, Baldo M, Lombardo U, Cugnon J, and Lejeune A 1998 *Phys. Rev. C* **57** 704
[11] Baldo M, Burgio G F, and Schulze H-J 2000 *Phys. Rev. C* **61** 055801; Schulze H-J, Polls A, Ramos A, and Vidaña I 2006 *Phys. Rev. C* **73** 058801
[12] Maessen P M M, Rijken T A, and De Swart J J 1989 *Phys. Rev. C* **40** 2226
[13] Stoks V G J and Rijken T 1999 *Phys. Rev. C* **59** 3009
[14] Vidaña I, Logoteta D, Providência C, Polls A, and Bombaci I 2011 *Europhys. Lett.* **94** 11002
[15] Burgio G F, Baldo M, Sahu P K, and Schulze H-J 2002 *Phys. Rev. C* **66** 025802
[16] Baldo M, Buballa M, Burgio G F, Neumann F, Oertel M, and Schulze H-J 2003 *Phys. Lett. B* **562** 153; Baldo M, Burgio G F, Castorina P, Plumari S, and Zappalà D 2007 *Phys. Rev. C* **75** 035804
[17] Maieron C, Baldo M, Burgio G F, and Schulze H-J 2004 *Phys. Rev. D* **70** 043010
[18] Kurkela A, Romatschke P, and Vuorinen A 2010 *Phys. Rev. D* **81** 105021
[19] Chodos A, Jaffe R L, Johnson K, Thorn C B, and Weisskopf V F 1974 *Phys. Rev. D* **9** 3471
[20] Witten E 1984 *Phys. Rev. D* **30** 272; Baym G, Kolb E W, McLerran L, Walker T P, and Jaffe R L 1985 *Phys. Lett. B* **160** 181; Glendenning N K 1990 *Mod. Phys. Lett. A* **5** 2197
[21] Fahri E and Jaffe R L 1984 *Phys. Rev. D* **30** 2379
[22] Alford M and Reddy S 2003 *Phys. Rev. D* **67** 074024
[23] Pirner H J, Chanfray G, and Nachtmann O 1984 *Phys. Lett. B* **147** 249; Drago A, Tambini U, and Hjorth-Jensen M 1996 *Phys. Lett. B* **380** 13
[24] Glendenning N K 1992 *Phys. Rev. D* **46** 1274
[25] Heiselberg H, 1993 *Phys. Rev. D* **48** 1418; Glendenning N K 2001 *Phys. Rep.* **342** 393
[26] Maruyama T, Chiba S, Schulze H-J, and Tatsumi T 2007 *Phys. Rev. D* **76** 123015; 2008 *Phys. Lett. B* **659** 192
[27] Maruyama T, Tatsumi T, Endo T, and Chiba S 2006 *Recent Res. Devel. in Physics* **7** 1
[28] Prakash M, Bombaci I, Prakash M, Ellis P J, Lattimer J M, and R. Knorren, 1997 *Phys. Rep.* **280** 1
[29] Nicotra O E, Baldo M, Burgio G F, and Schulze H-J 2006 *Astron. Astrophys.* **451** 213; Nicotra O E, Baldo M, Burgio G F, and Schulze H-J 2006 *Phys. Rev. D* **74** 123001
[30] Burgio G F and Schulze H-J 2009 *Phys. Atom. Nuc.* **72** 1197
[31] Burgio G F and Schulze H-J 2010 *Astron. Astrophys.* **518** A17
[32] Burgio G F, Schulze H-J, and Li A 2011 *Phys. Rev. C* **83** 025804
[33] Pons J A, Reddy S, Prakash M, Lattimer J M, and Miralles J A 1999 *Astrophys. J.* **513** 780
[34] Strobel K and Weigel M K 2001 *Astron. Astrophys. Suppl.* **367** 582
[35] Bloch C and De Dominicis C 1958 *Nucl. Phys.* **7** 459; 1959 *ibidem* **10** 181,509
[36] Baldo M and Ferreira L S 1999 *Phys. Rev. C* **59** 682
[37] Vidaña I, Bombaci I, Polls A, and Ramos A 2003 *Astron. Astrophys.* **399** 687
[38] Demorest P B, Pennucci T, Ransom S M, Roberts M S E, and Hessels J W T 2010 *Nature* **467** 1081